New Phytologist

The tonoplast localized protein PtNPF1 participates in the regulation of nitrogen response in diatoms

Anna Santin[1], Monia Teresa Russo[1], Laura Morales de los Ríos[2], Maurizio Chiurazzi[3], Maurizio Ribera d'Alcalà[1], Benoît Lacombe[2], Maria Immacolata Ferrante[1,4] and Alessandra Rogato[1,3]

[1]Stazione Zoologica Anton Dohrn, Villa Comunale, Naples, 80121, Italy; [2]Institute for Plant Science of Montpellier (IPSiM), University of Montpellier, CNRS, INRAE, Montpellier SupAgro, Place Pierre Viala 2, Montpellier, 34060, France; [3]Institute of Biosciences and BioResources, CNR, Via P. Castellino 111, Naples, 80131, Italy; [4]National Institute of Oceanography and Applied Geophysics, Trieste, 34010, Italy

Authors for correspondence:
Alessandra Rogato
Email: alessandra.rogato@ibbr.cnr.it

Maria Immacolata Ferrante
Email: mariella.ferrante@szn.it

Received: *26 October 2023*
Accepted: *21 November 2023*

New Phytologist (2024) **241:** 1592–1604
doi: 10.1111/nph.19461

Key words: diatom NPFs, genome editing, luxury uptake, nitrogen, *Phaeodactylum tricornutum*, vacuole.

Summary

- Diatoms are a highly successful group of phytoplankton, well adapted also to oligotrophic environments and capable of handling nutrient fluctuations in the ocean, particularly nitrate. The presence of a large vacuole is an important trait contributing to their adaptive features. It confers diatoms the ability to accumulate and store nutrients, such as nitrate, when they are abundant outside and then to reallocate them into the cytosol to meet deficiencies, in a process called luxury uptake.
- The molecular mechanisms that regulate these nitrate fluxes are still not known in diatoms. In this work, we provide new insights into the function of *Phaeodactylum tricornutum* NPF1, a putative low-affinity nitrate transporter. To accomplish this, we generated overexpressing strains and CRISPR/Cas9 loss-of-function mutants.
- Microscopy observations confirmed predictions that PtNPF1 is localized on the vacuole membrane. Furthermore, functional characterizations performed on knock-out mutants revealed a transient growth delay phenotype linked to altered nitrate uptake.
- Together, these results allowed us to hypothesize that PtNPF1 is presumably involved in modulating intracellular nitrogen fluxes, managing intracellular nutrient availability. This ability might allow diatoms to fine-tune the assimilation, storage and reallocation of nitrate, conferring them a strong advantage in oligotrophic environments.

Introduction

The variation of nutrient availability due to factors such as depth, turbulence and tides plays a crucial role in the functioning of highly dynamic marine ecosystems (Tuerena *et al.*, 2019; Tsutsumi *et al.*, 2020). Nutrient scarcity acts as a selective pressure for all living organisms and a flexible and highly regulated balance between environmental and intracellular nutrients allows to handle nutrient variability (Efeyan *et al.*, 2015).

In scenarios of intermittent availability, diatoms, unicellular photosynthetic organisms that represent one of the most diverse groups of phytoplankton, own an adaptive feature which gives them an ecological advantage. This solution is represented by nutrient storage capacity (Kooistra *et al.*, 2007; Behrenfeld *et al.*, 2021). In particular, nitrate (NO_3^-) in excess, taken up in response to immediate nutritional demands, can be accumulated inside the cell during favourable periods, a phenomenon also called 'luxury uptake', and can be reallocated and assimilated when environmental NO_3^- is scarce, spatially confined or temporarily unavailable (Shebanova *et al.*, 2017; Wang *et al.*, 2019; Behrenfeld *et al.*, 2021). This ability confers diatoms a particularly useful trait in fluctuating and oligotrophic environments (Stief *et al.*, 2022). For example, in dark and anoxic conditions, some diatoms can consume 84–87% of their intracellular NO_3^- pool within 1 day through the Dissimilatory NO_3^- Reduction to Ammonium (NH_4^+), an anaerobic respiration process used by many microbes to enter a resting stage for long-term survival (Kamp *et al.*, 2011).

However, accumulation of nutrients such as NO_3^- in the directly bioavailable form is not possible, as their high levels can be toxic in the cytoplasm (Gerasimaitė *et al.*, 2014; Shebanova *et al.*, 2017). For this reason, diatoms take up and store NO_3^- in the vacuole. In fact, they host large internal vacuoles that act as a nutrient storage site, similar to higher plants (Kooistra *et al.*, 2007; Behrenfeld *et al.*, 2021). When NO_3^- uptake exceeds immediate nutritional demands, it can be accumulated inside the vacuole, reaching concentrations of up to 100 mM, several orders of magnitude higher than ambient NO_3^- concentrations (Kamp *et al.*, 2011).

Vacuoles are membrane-bound organelles that contain inorganic ions and organic compounds. Their morphology and biochemistry, as well as the materials they store, vary greatly depending on the cell type and stage (Noguchi & Hayashi, 2014). The vacuolar membrane, also called tonoplast, contains transport

proteins with different functions, which are often considered key players in mechanisms of molecules storage in and release from the vacuolar environment (Behrenfeld *et al.*, 2021).

The mechanisms controlling the vacuole functioning in diatoms are still poorly known, and also the function of many proteins localized on the tonoplast needs to be characterized.

Recent genomic and genetic developments have enabled the identification and functional characterization of few vacuolar proteins in diatoms. Huang *et al.* (2016) found two 1,6-β-transglycosylases responsible for synthesizing and transporting chrysolaminarin, the main storage carbohydrate of diatoms, located on the tonoplast. Dell'Aquila *et al.* (2020) discovered that the vacuolar transport chaperone complex localizes on the tonoplast, suggesting a possible role in phosphorus influx/efflux in the diatom vacuole, but does not relocate from the nuclear envelope/endoplasmic reticulum to the vacuole during phosphate limitation, as shown before in plants. However, many other vacuolar transporters are still considered orphan proteins.

The diatom putative low-affinity NO_3^- transporters NPFs (diNPFs) have proven to be a very diverse and interesting class of transporters. Phylogenetic analyses reveal that they diverge into two clades, and 25% of diNPFs, all belonging to Clade II, were predicted to be tonoplast-located (Santin *et al.*, 2021).

Here, we provide new insights into diNPFs Clade II and on their role within cellular metabolism. To our knowledge, this is the first characterization of a member of this gene family in diatoms. For this purpose, *Phaeodactylum tricornutum* was chosen as model organism. This pennate diatom is well-characterized in terms of functional genomics, and many innovative genomic and genetic resources became recently available, such as the CRISPR/-Cas9 genome editing technology (Nymark *et al.*, 2016; Russo *et al.*, 2022). *Phaeodactylum tricornutum* owns two diNPFs, of which one, PtNPF1, belongs to Clade II (Santin *et al.*, 2021).

By conducting molecular and functional genetic analyses, we provide support to the hypothesis that the *PtNPF1* gene could be involved in regulating N dynamics in diatom cells, helping to explain the unique ability and plasticity of these successful microalgae to store and reallocate intracellular N in response to variable conditions.

Materials and Methods

Phaeodactylum tricornutum culture conditions

An axenic culture of *P. tricornutum* Bohlin, CCMP 632, was obtained from the Provasoli-Guillard National Centre for Culture of Marine Phytoplankton. The culture was maintained in F/2 medium without silica (Guillard, 1975), at 18°C and white light of 90 µmol photons m^{-2} s^{-1} was provided at a 12 h : 12 h, light : dark cycle.

In silico prediction of PtNPF1 vacuole targeting

FIMO v.5.4.1 (https://meme-suite.org/meme/tools/fimo) was used to search in the PtNPF1 sequence the conserved motif [D/E] XXXL[L/I] for vacuole localization previously identified by Bonifacino & Traub (2003).

Generation of *PtNPF1* overexpressing lines

The full-length *PtNPF1* gene (Phatr3_J47148) coding sequence was fused to the *YFP* gene at its 5′ end or with *GFP* gene at its 3′ end. The two constructs were generated using the Gibson assembly method (Gibson *et al.*, 2009, 2010) following the manufacturer's instructions. For *PtNPF1-YFP*, the PtLhcf2pPtovoAyfp plasmid (Russo *et al.*, 2023), containing the Light Harvesting Complex protein family F2 promoter (*Lhcf2*p), was used as backbone, for *PtGFP-NPF1*, the PmH4pH4N-GFP plasmid (Sabatino *et al.*, 2015), containing the *Pseudo-nitzschia multistriata* histone *H4* promoter (*PmH4*p), was used as backbone.

Details of oligonucleotides are listed in Supporting Information Table S1.

P. tricornutum cells were transformed with a two-vector system as reported by Falciatore *et al.* (1999). Transformed cells were tested for the presence of the transgene by colony PCR (see Table S1 for primer sequences).

Confocal microscopy and morphological parameters analyses

Subcellular localization analysis was performed using a Leica SP8 X confocal laser-scanning microscope, using the HC PL APO CS2 63X/1.20 water objective. Chlorophyll *a* autofluorescence was excited at 554 nm and detected at 650–741 nm. YFP/GFP fluorescence was excited at 488 nm and detected at 500–562 nm. Vacuoles in *P. tricornutum* wild-type (WT) and knock-out strains were detected using a green fluorescent vacuolar membrane marker MDY-64 as described by Huang *et al.* (2016). Cells were visualized by excitation at 451 nm and detection at 490–562 nm. For each cell, the number of vacuoles was counted and their area was measured using IMAGEJ (FIJI; Schindelin *et al.*, 2012). The ratio between the total area of vacuoles and the total area of the cell was calculated.

Generation of *PtNPF1* knock-out mutants

Guide RNAs (gRNAs) were obtained using the CRISPOR tool (http://crispor.gi.ucsc.edu/) (Haeussler *et al.*, 2016), based on the Moreno-Mateos score and allowing the prediction of specific genomic sites along with the exclusion of predictable off-targets. The two crRNA sequences designed on *PtNPF1* (gNPF1_a and gNPF1_b) cover the 715th–1124th-bp region of the *PtNPF1* gene, which corresponds to the 238th–374th-aa region of the PtNPF1 protein sequence, including four transmembrane helices (Fig. S1a; Table S1). The crRNAs on the selective gene *PtAPT* were chosen from Serif *et al.* (2018; Table S1). Duplexes of designed crRNAs and universal tracrRNA were prepared following the manufacturer's instructions. *In vitro* CRISPR-Cas9 ribonucleoprotein (RNP) cleavage assay was performed as described in Russo *et al.* (2022; Fig. S1b). Ribonucleoprotein complexes were assembled following Serif *et al.* (2018) and delivered to wild-type cells by particle bombardment (Falciatore *et al.*, 1999).

Transformed colonies and four WT colonies were picked and lysed as described in Daboussi *et al.* (2014) and genotyped using Sanger sequencing (see Table S1 for primer sequences).

N starvation and repletion experiment

Phaeodactylum tricornutum WT and knock-out lines growing axenically to mid-exponential phase were diluted to 2×10^5 cells ml^{-1} and transferred in F/2 medium without silica with 50 μM $NaNO_3$ for 4 d and then resupplied with 882 μM $NaNO_3$. The same experiment was performed by repleting cells with 882 μM NH_4Cl or 882 μM urea as alternative N sources. Moreover, cells were starved with no P and then resupplied with 36 μM $NaH_2PO_4 \cdot H_2O$. Each condition was set up in triplicate. The cell concentration was evaluated through *in vivo* chlorophyll *a* fluorescence, a proxy for growth, measured through a multifunctional monochromator-based microplate reader (Infinite™ M1000 Pro; Tecan, Palm Springs, CA, USA), and confirmed through the flow cytometer BD FACSVerse™ (BD Biosciences, San Jose, CA, USA).

To analyse extra- and intracellular NO_3^- pools, 4×10^7 cells were filtered and NO_3^- content was extracted according to McCarthy *et al.* (2017). NO_3^- in the extract and in the filtrate was measured by UV spectrophotometry (Cary 100 UV–Vis spectrophotometer – Varian Inc., Cary, NC, USA, single-beam spectrophotometer) at a wavelength of 220 nm, and correlated to a NO_3^- standard curve (NO_3^- concentrations from 5 to 800 μM in N-free F/2 medium), according to McCarthy *et al.* (2017).

For gene expression analyses, cells were collected at four time points: at the mid-exponential phase at the beginning of the experiment (Day 0 in the graphs), after 4 d of growth in NO_3^- starvation (Day 4), after 1 (Day 5) and 3 (Day 7) days after NO_3^- repletion.

To determine whether there were significant differences between the different strains and during time, a two-way ANOVA with Tukey's multiple comparison test was performed, and statistics for time, strain and interaction were recorded. Statistics was performed using GraphPad Prism v.6.0.

RNA extraction and qPCR

RNA extraction and gene expression analysis were performed as described in Santin *et al.* (2021). Fold changes were obtained with the Relative Expression Software Tool-Multiple Condition Solver (REST-MCS; Pfaffl *et al.*, 2002), and values above ±2 were considered significant (see Table S1 for primer sequences).

Results

PtNPF1 subcellular localization

In both higher plants and diatoms, a conserved di-leucine-based motif, [D/E] XXX L[L/I] (Bonifacino & Traub, 2003), has been identified as being involved in the localization to the tonoplast (Park *et al.*, 2013; Schreiber *et al.*, 2017). PtNPF1 contains the residues [EHAPLL] at the N-terminus, from the amino acid 16 to 21 (Fig. S2).

In order to experimentally confirm the PtNPF1 subcellular localization, a N-terminal green fluorescent protein (GFP) and a C-terminal yellow fluorescent protein (YFP) fused to PtNPF1 (PtNPF1-YFP and GFP-PtNPF1) were expressed in *P. tricornutum* cells. A total of 60% of the transformant clones showed the whole *PtNPF1-YFP* cassette insertion (Fig. S3). For two of these, *PtNPF1-YFP* overexpressing (OE) clones 4 and 9, the *PtNPF1* gene expression levels were measured: OE 4 showed a 5.12 ± 0.27-fold increase, while OE 9 showed a 4.21 ± 0.21-fold increase, compared with WT (Fig. 1a).

As shown in Fig. 1(b), confocal imaging confirmed PtNPF1 tonoplast localization. This localization pattern was observed in independent *PtNPF1-YFP* and *GFP-PtNPF1* OE strains (Figs 1b, S4b). Wild-type cells were stained with the tonoplast marker MDY-64 as control, to confirm localization (Huang *et al.*, 2018; Fig. 1c), because similar emission wavelengths did not allow co-localization between the fluorescent tag and MDY-64 staining.

Preliminary experiments to assess PtNPF1 capability to transport NO_3^- in a heterologous system were not conclusive (Methods S1; Fig. S5).

Vacuole morphology in N starvation and different N sources

Phaeodactylum tricornutum holds vacuolar-like structures comparable to plants. In particular, cells own two or more vacuoles, higher is their number smaller is their size, covering around half of the total cellular area (Fig. 2; Table S2). To test whether NO_3^- availability had a role in vacuole dynamics, the size and the number of the vacuoles in *P. tricornutum* WT cells grown, respectively, in normal and low NO_3^- concentrations (882 and 50 μM) for 4 d were examined, as well as the ratio between vacuole and total cell areas. The number of vacuoles did not vary between the two different growth conditions, with values of 3.48 ± 1.74 in normal conditions and 3.69 ± 1.40 in N starvation ($P = 0.6137$; Fig. 2e). Similarly, the ratio between vacuole and total cell areas did not significantly change, with *c.* 54% ± 9 of the cell volume occupied by vacuoles in normal conditions and *c.* 58% ± 13 in N starvation ($P = 0.1204$; Figs 2f, S6). However, intracellular NO_3^- content showed a significant reduction from 1.23 ± 0.04 pg per cell in normal conditions to 0.42 ± 0.07 pg per cell in N starvation condition, consistent with the cellular consumption ($P < 0.001$; Fig. 2g).

Intracellular NO_3^- content strongly represents vacuolar NO_3^- content. Since high NO_3^- levels are toxic in the cytoplasm (Gerasimaitė *et al.*, 2014; Shebanova *et al.*, 2017), NO_3^- taken up from the environment is quickly assimilated and converted to nitrite (NO_2^-) by an efficient nitrate reductase (McCarthy *et al.*, 2017) or stored into the vacuole (Kooistra *et al.*, 2007; Behrenfeld *et al.*, 2021; Stief *et al.*, 2022).

The intracellular NO_3^- content of *P. tricornutum* WT was also measured in cells grown in the presence of NH_4^+ as an alternative N source in the medium, to evaluate the preference of *P. tricornutum* for N sources utilization. In particular, cells growing until the exponential phase in normal medium supplemented with NO_3^-, were shifted in NO_3^-, as control, and in NH_4^+ for 4 d. The intracellular NO_3^- concentration did not change between the two environmental conditions, suggesting that cells preferred to uptake N from the external environment when

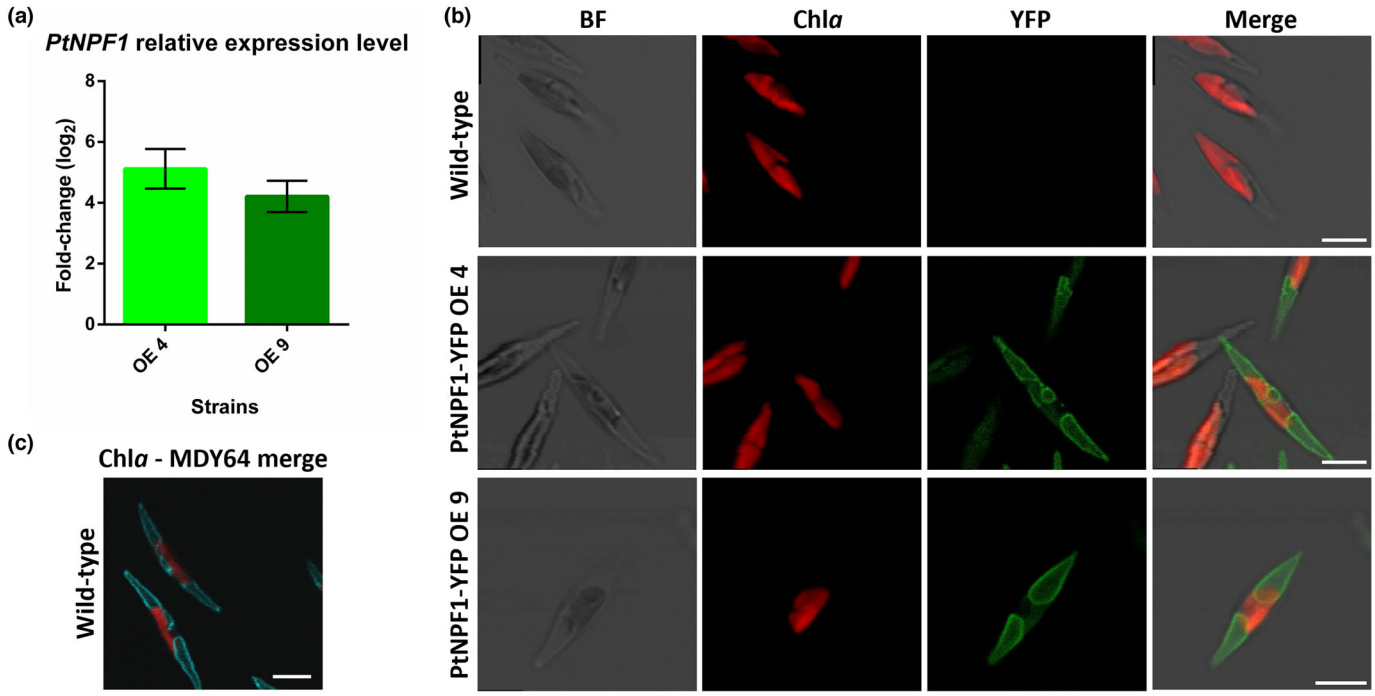

Fig. 1 Subcellular localization of PtNPF1 in overexpressing (OE) strains. (a) *PtNPF1* relative gene expression levels of *Phaeodactylum tricornutum* OE strains 4 and 9, compared with wild-type (WT) set as zero. Error bars represent the standard deviation of three technical replicates of two biological replicates. (b) Subcellular localization of the PtNPF1-YFP fusion protein in *P. tricornutum*, observed through confocal microscopy. From left to right: bright field images in grey, chlorophyll *a* fluorescence in red, YFP fluorescence in green and the merged image. Bar, 5 μm. (c) *P. tricornutum* WT cells stained with the vacuole tracker MDY-64. Merged image showing chlorophyll *a* in red and MDY-64 fluorescence in cyan. Bar, 5 μm.

available, regardless of the source, while maintaining intracellular N stored (Figs 2h, S7).

Ptnpf1 knock-out phenotype in response to N repletion

In order to investigate the physiological function of *PtNPF1*, *Ptnpf1* knock-out mutants were generated by using an optimized CRISPR/Cas9 gene editing system (Serif *et al.*, 2018; Russo *et al.*, 2022). Two independent *Ptnpf1* knock-out strains (KO 2.8 and KO 2.9), showing frameshift mutations, were selected and sequenced: KO 2.8 bears an insertion of 214-bp and a deletion of 403 bp on the two alleles, respectively, while KO 2.9 presents two deletions of 403 and 650 bp (Figs 3a,b, S8). Mutations of both KO clones caused frameshifts and/or stop codon insertion. These mutations resulted in the production of truncated proteins lacking transmembrane helices which, as a consequence, are unable to fold and function correctly (Figs 3c,d, S8).

To assess the physiological effects of *PtNPF1* knock-out in *P. tricornutum*, a series of experiments were conducted utilizing WT strain and the KO mutants 2.8 and 2.9, together with a *PtNPF1-YFP* OE strains.

Different *P. tricornutum* strains were grown in the presence of different NO_3^- concentrations (882 and 50 μM) and different N sources (882 μM NO_3^-, 882 μM NH_4^+ and 882 μM urea), and in accordance with Santin *et al.* (2021), no growth differences were observed in the analysed strains (Fig. S9), suggesting that PtNPF1 is not directly involved in the uptake of NO_3^- from the external environment into the cell. Furthermore, vacuole morphology was studied in *P. tricornutum* WT, *PtNPF1* OE strains and *Ptnpf1* knock-out mutants grown under normal and N-starved conditions. However, no differences in vacuole number or size were detected between the WT and mutant strains, regardless of the growth conditions (Fig. S6). In addition, the same response of WT to NH_4^+ as an alternative N source was observed in *P. tricornutum* transgenic lines (Fig. S7).

The phenotypical response to a N starvation and repletion experimental condition was compared in WT and *Ptnpf1* knock-out strains. After 4 d of growth in a medium with 50 μM NO_3^-, WT and *Ptnpf1* mutants were supplemented with 882 μM NO_3^-. No growth differences were observed between different strains during N starvation, whereas after NO_3^- repletion, both KO 2.8 and 2.9 showed a growth delay compared with WT (Fig. 4a,c).

This response is specific to the two analysed *Ptnpf1* knock-out mutants. Notably, PtNPF1 OE strains and a control knock-out for a different gene (Fig. S10a–e), generated using the same technique but with a different gene as target, did not exhibit any altered phenotype and behave similarly to the WT strain. This suggests that the observed phenotype is directly associated with the disruption of the gene of interest, rather than being an artifact of the genetic technique employed or the alteration of the *PtAPT* selection gene.

Moreover, to explain the growth delay of knock-out mutants, extra- and intracellular NO_3^- was measured. Results shown in Fig. 4(d,e) highlighted a clear-cut reduction in external NO_3^- concentration and a slower increase in the intracellular NO_3^-

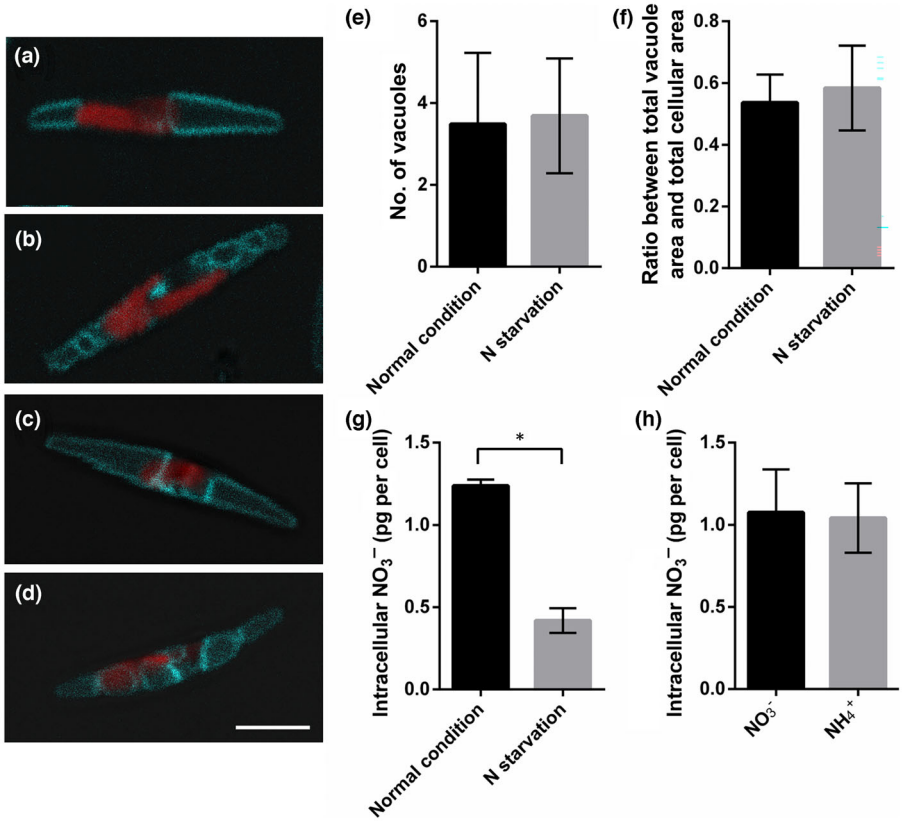

Fig. 2 Morphological parameters and intracellular NO_3^- content of *Phaeodactylum tricornutum* wild-type cells in the presence of different N concentrations and sources. (a–d) *P. tricornutum* observed through confocal microscope after 4 d under normal N (a) and (b), and N starvation conditions (c, d). Merged images showing chlorophyll *a* in red and tonoplast tracker MDY-64 in cyan. Bar, 5 μm. (e) Number of vacuoles and (f) ratio between total vacuole area and total cellular area. The values are shown as mean ± SD (N = see Supporting Information Table S2). (g) Intracellular NO_3^- content in *P. tricornutum* cells grown under normal N and N starvation conditions. (h) Intracellular NO_3^- content in *P. tricornutum* cells grown in NO_3^- and NH_4^+ as alternative N sources in the medium. The values are shown as mean ± SD ($n = 3$ biological replicates analysed for intracellular NO_3^- content per each condition). *, $P < 0.001$ resulting from the one-way ANOVA performed.

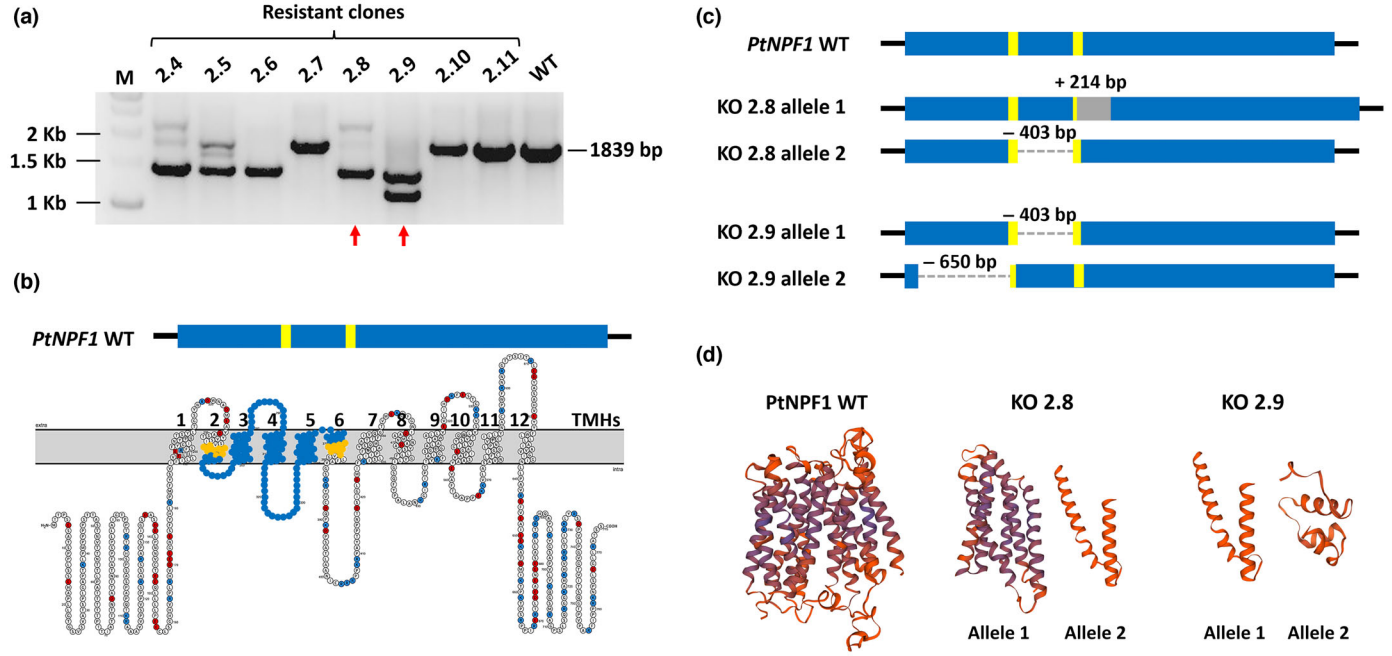

Fig. 3 Screening of *Ptnpf1* knock-out mutants. (a) Agarose gels showing the PCR screening of the *PtNPF1* gene on *Phaeodactylum tricornutum* wild-type (WT) and transformed cells positive to selection, M represents the molecular marker. (b) gRNAs designed on *PtNPF1* gene sequence (yellow boxes on the blue bar) and correspondence to transmembrane helices in folded PtNPF1 protein. In the bottom panel, blue dots indicate transmembrane helices included between gRNAs corresponding regions, represented by orange dots. TMHs indicate transmembrane helices. (c) *P. tricornutum* WT and knock-out mutants representation of Cas9 different cuts: KO 2.8 and 2.9 insertions and deletions on both alleles shown, respectively, in grey boxes and grey dotted lines. (d) Models of the PtNPF1 WT protein structure and of the truncated proteins in KO 2.8 and 2.9, resulting from mutations on both alleles. Smaller yellow, red and dark blue dots represents specific amino acids, respectively cysteines, aspartic/glutamic acids and arginines/lysines.

content in both the KO stains as compared to WT at 5 d after the transfer (Fig. 4d,e). In addition, the internal NO_3^- content stabilized at a higher level than the control. It is worth noting that the final difference in the internal stock between the mutants and the controls remained the same as observed in the initial conditions. Furthermore, for all the strains, this difference was practically equal to that of initial repleted conditions (Fig. 4e).

Other starvation and repletion experiments were performed, using P, NH_4^+ or urea as alternative nutrients. Results showed no growth differences between the strains after P starvation and repletion (Fig. 5b). Interestingly, a growth phenotype similar to NO_3^- starvation and repletion (Fig. 5a) was observed in *Ptnpf1* knock-out mutants when NH_4^+ or urea were added instead of NO_3^- during the repletion phase (Fig. 5c,d). These findings suggest a N-specific response that is not dependent on the environmental N source.

In order to find a mechanistic model for explaining the N-related growth delay, we analysed the expression profiles of a number of selected genes in response to the N starvation and repletion conditions in WT and mutated genetic backgrounds. The expression of another member of the NPF family, *PtNPF2*, did not significantly vary between different strains and over time, both in WT and in *Ptnpf1* knock-out strains (Fig. 6a). This means that the absence of one of the *PtNPFs* is not compensated by an alteration of the expression levels of the other one, suggesting no redundancy between the two *PtNPF* genes. Also, the expression levels of the *PtCLC3* gene, encoding for a putative vacuolar chloride channel, displayed no differences between strains during the NO_3^- starvation and repletion treatments (Fig. 6b).

Moreover, the expression levels of predicted high-affinity NO_3^- transporters (*PtNRT2s*) were evaluated. Two out of the three *PtNRT2s* predicted to the tonoplast, Pt40691 and Pt2171 (Table S3), did not show significant differences in the expression profiles between different strains (Fig. 6d,e). Interestingly, the tonoplast-predicted Pt54560 (Table S3) showed a progressive, significant induction in both WT and mutant strains during the N starvation treatment with a peak of expression at d4, but a faster decrease in the fold-change expression was then observed in WT, as compared to mutant cells that maintained high expression levels up to d5 (Fig. 6c). The same profile was observed for two out of three *PtNRT2s* predicted to the plasma membrane, Pt26029 and Pt54101 (Table S3), progressively upregulated in all strains at d4, and then showing a faster reduction in expression levels in WT that was not observed in KO mutants after N repletion at d5 (Fig. 6f,g). Pt2032, predicted to the plasma membrane (Table S3), did not show significant differences between strains over time (Fig. 6h).

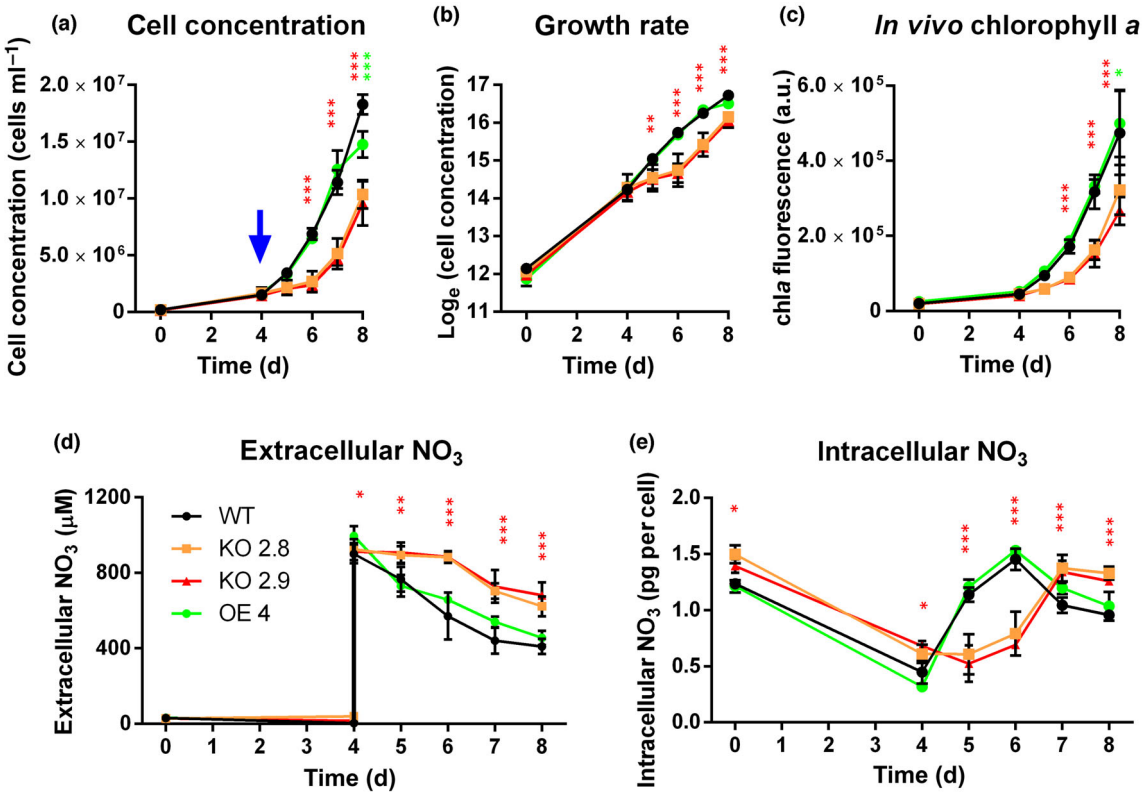

Fig. 4 Growth phenotype in *P. tricornutum* wild-type (WT) and *Ptnpf1* knock-out mutants. (a) Cell concentration, (b) natural logarithm of growth curves and (c) measurement of *in vivo* chlorophyll *a* autofluorescence, providing a proxy for growth, for the WT, KO 2.8 and 2.9 knock-out mutants and one OE4 overexpressing strain (d) Extracellular NO_3^- removed from the media by WT and *Ptnpf1* knock-out cells measured by UV spectrophotometry. (e) Intracellular NO_3^- extracted from cells and measured by UV spectrophotometry. The blue arrow indicates the NO_3^- repletion day. The values are shown as mean ± SD ($n = 3$ biological replicates). *, $P < 0.05$; **, $P < 0.01$; ***, $P < 0.001$ resulting from the two-way ANOVA performed.

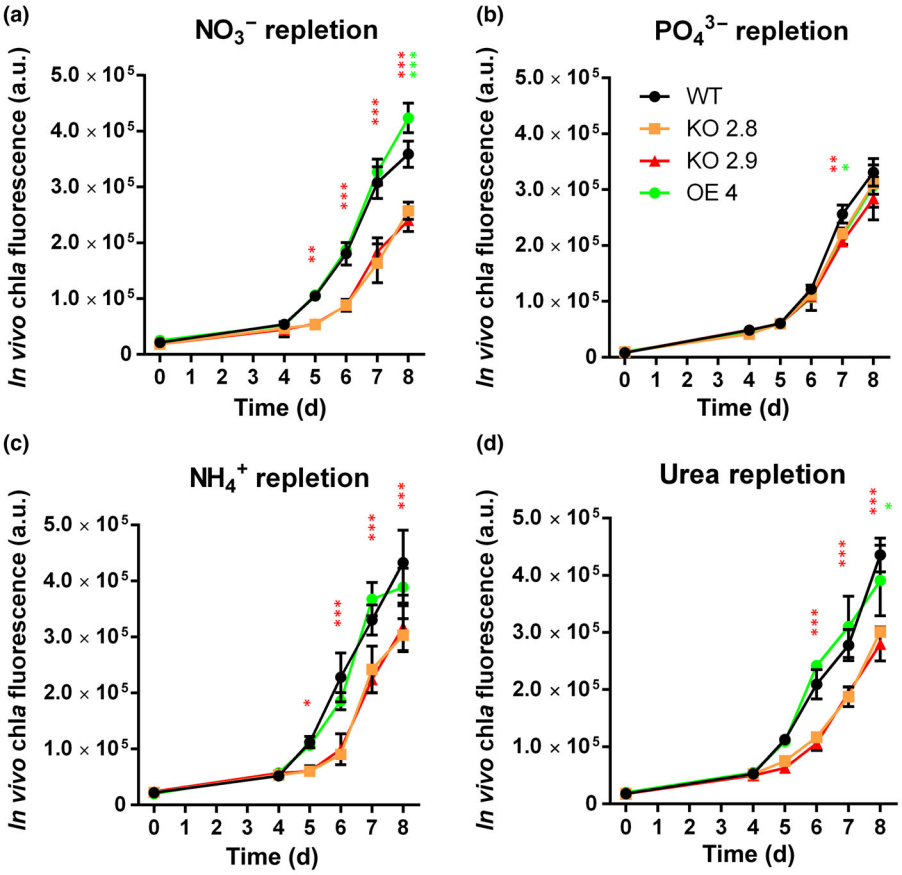

Fig. 5 P and N starvation and repletion experiments on *Phaeodactylum tricornutum* wild-type (WT) and *Ptnpf1* knock-out mutants. (a) Starvation with 50 μM $NaNO_3$ and repletion with 882 μM $NaNO_3$. (b) Starvation with no P and repletion with 36 μM $NaH_2PO4{\cdot}H_2O$. Starvation with 50 μM $NaNO_3$ and repletion with 882 μM NH_4Cl (c) and 882 μM urea (d). *In vivo* chlorophyll *a* fluorescence was used for measurements as proxy for growth. Experiments were performed on WT, KO 2.8 and 2.9 knock-out mutants and one OE4 overexpressing strain. The values are shown as mean ± SD ($n = 3$ biological replicates). *, $P < 0.05$; **, $P < 0.01$; ***, $P < 0.001$ resulting from the two-way ANOVA performed.

In addition, the profiles of expression of the nitrate reductase *PtNR* and the nitrite transporter *PtNAR1* displayed no differences between strains during the NO_3^- depletion/repletion treatments (Fig. 6i,j). These results suggested a specific cross-talk between *PtNPF1* and the high-affinity NO_3^- transporters in regulating the intracellular reallocation of the nutrient.

Discussion

There are several evidences that diatoms can effectively respond to variations in nutrient availability, especially in dissolved inorganic nitrogen (DIN; Rosenwasser *et al.*, 2014; Smith *et al.*, 2019).

During periods of nonlimiting N availability, diatoms accumulate in the vacuole mainly NO_3^-, as a consequence of luxury uptake, and then, in response to N deficiency, they allow NO_3^- to be newly available for the cell metabolism (Lomas & Glibert, 2000; Stief *et al.*, 2013; Bender *et al.*, 2014). This seems to be one of the adaptive roles of the vacuole in diatoms (Kooistra *et al.*, 2007), similar to other organisms like plants (He *et al.*, 2017). However, the mechanisms and the regulation of NO_3^- trafficking between vacuole and cytosol remain still elusive in diatoms.

The presence of putative low-affinity NO_3^- transporters in addition to high-affinity transporters for NH_4^+ and NO_3^-, which are more suited for the typical N concentrations present in the ocean, raises several questions on their location and function. NH_4^+ transporters (AMT) are all predicted to be plasma membrane-located (Busseni *et al.*, 2019), while both NO_3^- transporters families (NRT2s and NPFs) are predicted to be distributed in the plasma membrane as well as in other cellular compartments, including tonoplast (Rogato *et al.*, 2015; Santin *et al.*, 2021).

In this study, we have analysed in detail localization and putative functions of one of the two predicted low-affinity NO_3^- transporters, named PtNPF1, using *P. tricornutum* as model diatom. PtNPF1 belongs to Clade II diNPFs, evolutionary and structurally close to higher plant NPFs (Santin *et al.*, 2021).

A vacuole targeting motif was identified in PtNPF1 amino acid sequence and localization analyses confirmed that the protein resides in the tonoplast (Fig. 1), the membrane which mediates the transport of various ions and metabolites between the vacuole and cytosol. First, we analysed the response of the vacuole as a whole to NO_3^- variations, by performing a microscopic analysis of the *P. tricornutum* vacuole morphology in response to N starvation and, differently to what was recently reported in response to phosphate deprivation (Dell'Aquila *et al.*, 2020), we did not observe differences in *P. tricornutum* vacuole, neither in number nor in size (Fig. 2a–f). Concomitantly, the intracellular NO_3^- content, mainly stored in the vacuole, dramatically decreased after the N starvation treatment (Fig. 2g), suggesting that the nutrient is reallocated through the efflux in the cytosol and assimilated.

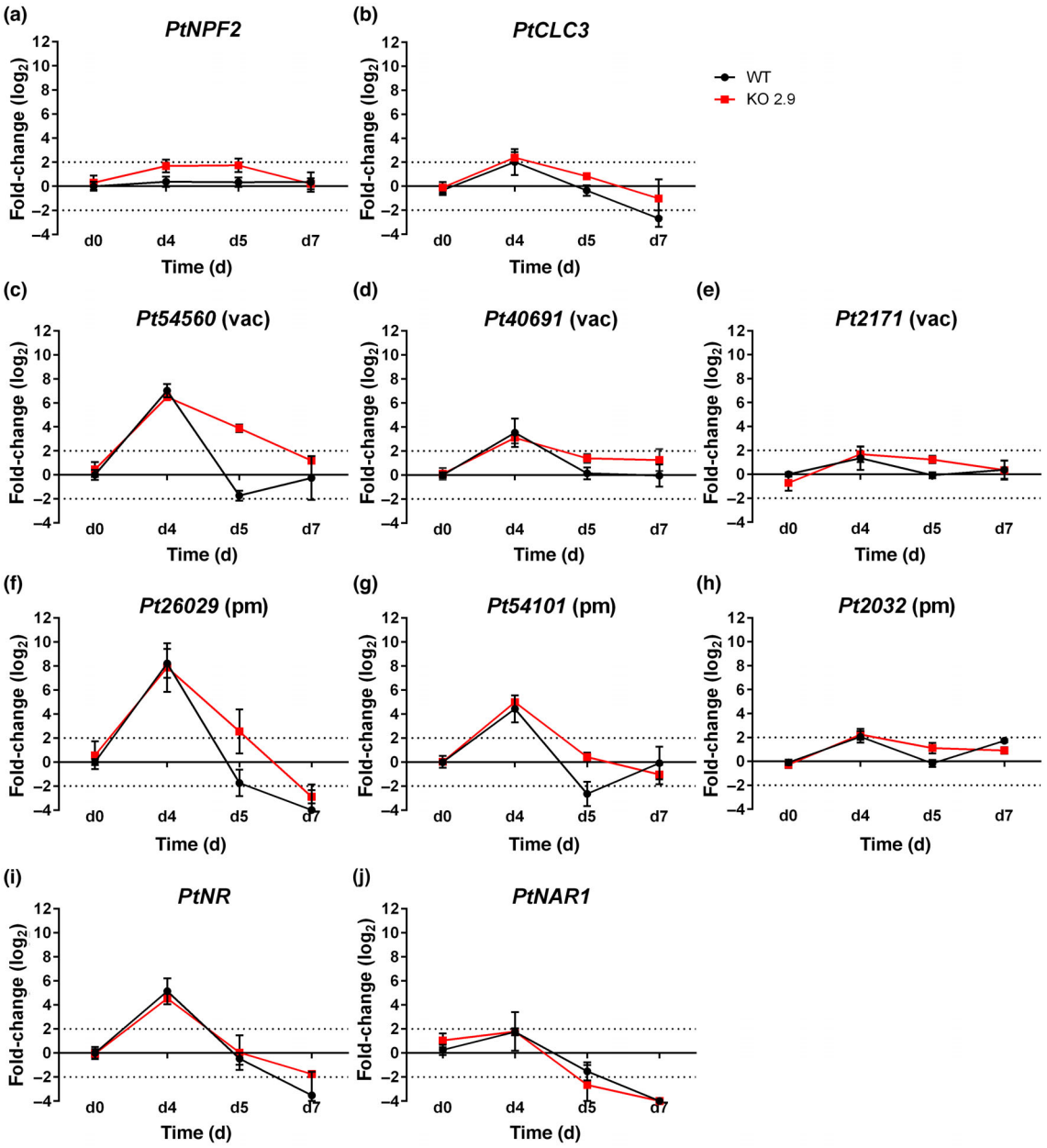

Fig. 6 Relative expression levels of genes involved in N transport and metabolism in *Phaeodactylum tricornutum* wild-type (WT) and *Ptnpf1* knock-out mutant KO 2.9 strains during N starvation and repletion experiment. d0 represents the beginning of the growth curve in N starvation, d4 indicates 4 d of N starvation, d5 1 d from N repletion and d7 3 d from N repletion. WT at d0 was set as reference condition, so as zero. The values are shown as mean ± SD (three technical replicates for $n = 2$ biological replicates). Values above ±2 were considered significant. (a) *PtNPF2*: another putative low-affinity NO_3^- transporter; (b) *PtCLC3*: putative vacuolar chloride channel; (c) Pt54560, (d) Pt40691 and (e) Pt2171: putative vacuolar (vac) high-affinity NO_3^- transporters; (f) Pt26029, (g) Pt54101 and (h) Pt2032: putative plasma membrane (pm) high-affinity NO_3^- transporters; (i) *PtNR*: NO_3^- reductase; (j) *PtNAR1*: NO_2^- transporter.

Since morphology is not affected, one possibility is that the changes in intracellular NO_3^- content, mainly vacuolar, lead to a different texture or biochemical composition of the vacuole (McCarthy *et al.*, 2017; Raven & Beardall, 2022), not detectable with confocal microscopy. In fact, the vacuole represents approximately half of the cell volume, and it also plays a critical role in osmotic regulation, predator defence and buoyancy control (Behrenfeld *et al.*, 2021). Therefore, a chemical modification rather than changes in vacuole size and number can be the consequence of a self-regulatory programme aimed to respond efficiently to sudden variation of nutritional demands (Raven & Beardall, 2022).

We also tested whether the cells supplied with NH_4^+ would elicit different responses in cellular DIN handling. It is energetically favourable for diatoms to meet their N requirements from NH_4^+ over NO_3^-, as the first is in the correct oxidation state for subsequent incorporation into nucleic acids, amino acids and proteins (Dortch, 1982; Dortch *et al.*, 1985). For this reason, among various inorganic N species, NH_4^+ is preferably taken up and directly consumed by phytoplankton (Mikaelyan *et al.*,

2015). However, many diatoms use a disproportionate fraction of total N as NO_3^- even when NH_4^+ is available in excess, reason why they are called NO_3^- opportunists (Lomas & Glibert, 2000; Glibert *et al.*, 2016). We observed that, when NH_4^+ rather than NO_3^- is given from the external environment, diatoms prefer to take it up from the medium while maintaining intracellular N stored so that intracellular NO_3^- does not vary in this condition (Fig. 2h). This supports the hypothesis that an equilibrium can be reached through co-provision of both NH_4^+ and NO_3^- (Glibert *et al.*, 2016), whose fine regulation can act in a synergistic way to induce growth. The capability of diatoms to cope not only with different N concentrations but also with different N sources, gives them an important advantage in their ecological niche and in the context of a changing world, dominated by different N forms enriching seawater through anthropogenic activities (Glibert *et al.*, 2016).

Anyhow, our hypothesis is that PtNPF1, in response to N starvation, plays a role in the re-mobilization of NO_3^- stored in the vacuole at high concentration (estimated up to 100 mM; Kamp *et al.*, 2011), to make it available again in the cytosol.

PtNPF1 transport function is supported by the structural homology with the plant AtNPF6.3 (Santin *et al.*, 2021). PtNPF1 is supposed to fold and insert in the tonoplast with the two ends located in the cytosol, suggesting a mechanism of transport of the substrate from the vacuole to the cytosol, and not in the opposite direction, for which two other transmembrane helices should be requested to overturn the protein (Yan *et al.*, 2013; Longo *et al.*, 2018). Furthermore, the predicted transmembrane helices (TMs) of the PtNPF1 structural model are 12 (Santin *et al.*, 2021). It has been observed that transporters with an even number of TMs had both C and N terminals on the cytoplasmic side of the membrane, while proteins with odd number of TMs had one end in cytoplasmic side and other in extracellular side (Kumar *et al.*, 2022). In this scenario, PtNPF1 could mediate NO_3^- efflux similarly to the *Arabidopsis thaliana* AtNPF5.11, AtNPF5.12 and AtNPF5.16 transporters, responsible of vacuolar NO_3^- release in the cytosol (He *et al.*, 2017).

Heterologous expression systems, such as *Xenopus laevis* oocytes, are commonly used to confirm transport activity, identify transported substrates, and assess substrate affinity and kinetics for many plant transporters (Miller & Zhou, 2000; Léran *et al.*, 2020).

While several predictions support PtNPF1 transport activity as a low-affinity NO_3^- transporter, from our first attempts, no transport activity was observed in oocytes injected with PtNPF1, and the conditions tested did not allow us to conclude that our protein is a NO_3^- transporter (Fig. S5). However, these results cannot be considered conclusive and exhaustive as, in heterologous expression experiments, lack of transport can be due to different technical reasons. Of particular relevance is that, for diatoms, the heterologous expression of transporters remains a challenge as these proteins have been so far poorly characterized (Hildebrand *et al.*, 1998; Knight *et al.*, 2016). More in-depth research and experiments are required to definitively confirm PtNPF1 transport activity for NO_3^- or any other potential substrates.

To further explore the potential of PtNPF1 while inferring its putative function, we generated knock-out mutants, using the CRISPR/Cas9 system coupled with proteolistics (Serif *et al.*, 2018; Russo *et al.*, 2022), confirming that this mutation approach is efficient and robust for gene editing in diatoms.

Growth kinetics of *P. tricornutum* WT and mutant strains on different N sources and different NO_3^- concentrations did not show differences, in accordance with the profile of expression observed for *PtNPF1* in previous research (Santin *et al.*, 2021). We then carried out a NO_3^- starvation and repletion experiment and observed a significant growth delay and a retarded NO_3^- uptake in two independent *Ptnpt1* knock-out mutants immediately after N repletion (Fig. 4a–e).

When N is present again in the environment after a deficiency period, NO_3^- flux inside the cell needs to be inverted, blocking vacuolar NO_3^- release and allowing NO_3^- uptake from external environment. Therefore, we infer that there is a coupling between the processes on the plasma membrane and those on the tonoplast, likely with key proteins that act as sensors and transfer the signal between different cell compartments, taking into account both the physiological conditions of the cell and the surrounding medium (Kamp *et al.*, 2011).

Absence of the growth delay phenotype between the strains after P starvation and repletion (Fig. 5b), while being observed independently of the external N source supplied (Fig. 5a–d), and the lack of N intake during the lag time, allow us to exclude the possibility that the response is triggered from the outside N concentration. This leads us to hypothesize that PtNPF1 might be involved in restarting or rerouting N metabolism, which reactivates the intake.

The growth delay of *Ptnpf1* mutants compared with WT cells, OE strains and knock-out mutants for a different gene, generated using the same technique and the same selection gene (Figs 4, S10), can be explained through the interruption of the signalling pathway that occurs between the intracellular N distribution and the vacuole, as an intermediate step to reactivate intake when environmental NO_3^- concentration increases. This is supported by the upregulation of three out of six *PtNRT2*s in the *Ptnpf1* mutants, not only during N starvation but also after N repletion. In particular, Pt54560, a *PtNRT2* predicted to the tonoplast, is upregulated both in WT and mutant backgrounds during N starvation (Fig. 6c). Then, in the *Ptnpf1* knock-out background, Pt54560 relative expression level after N repletion, although slightly reduced as compared to N starvation, is still significantly higher than in WT cells up to d5, suggesting that the mutants still prefer to transiently reallocate vacuolar NO_3^- rather than taking up the extracellular one. Since signalling pathways and ion fluxes are still poorly understood in diatoms (Smith *et al.*, 2019; Jaubert *et al.*, 2022; Helliwell, 2023), reconstructing these processes is one of the main challenges, as well as testing whether PtNPF1 could play a role in this context, similarly to what observed in higher plants' NPFs, acting as both sensors and transporters (Gojon *et al.*, 2011).

The slower regulation of *PtNRT2s* in *Ptnpf1* mutants compared with WT, parallel to the delay in NO_3^- accumulation after

repletion, could also have another explanation. There could be a common mechanism controlling both NO_3^- influx and *PtNRT2* gene expression, similar to higher plants NRT2s (Fraisier *et al.*, 2000; Pii *et al.*, 2016). They have a two-level control: a post-translational control mainly based on the accessory protein NAR2 protein synthesis (Pii *et al.*, 2016) and post-transcriptional events affecting abundance and/or activity of the NRT2 proteins, such as the regulation of transcript stability (Laugier *et al.*, 2012). Since diatom genomes do not encode for NAR2 (Rogato *et al.*, 2015), it is possible that PtNRT2s are under a post-transcriptional control, which could play a role in their response to environmental cues and could explain the similar trend in responses in transcript levels of *PtNRT2* genes and NO_3^- influx.

An unbalanced regulation of NO_3^- transport system, but not a different regulation of N assimilation pathway, has been observed in *Ptnpf1* mutants after N repletion, suggesting again that different regulators can play a role in controlling N fluxes and metabolism inside the cell (Fig. 6i,j). This is well known for higher plants, with many components, such as transporters, receptors, second messengers and transcription factors, localized in different cellular compartments or free to move between them, involved in mediating short- and long-term metabolic responses to N (Lamig *et al.*, 2022).

Moreover, despite the delay in growth and N uptake as well as a slower regulation of two *PtNRT2* expression levels, after 4 d from N repletion all the strains reached the same physiological condition, indicating the phenotype observed was transient and other mechanisms occurred to shape diatom metabolism. A similar response was previously observed by Tan (2020) with a delayed recovery of photosynthetic efficiency after N resupply, in the knock-out mutants of the putative high-affinity NO_3^- transporter Pt26029. This is probably due to redundancy of key players regulating N transport and metabolism in diatoms. Based on the results described here, redundancy or degeneracy (Edelman & Gally, 2001) of NO_3^- transporters active at different substrate concentrations and localized in different compartments, could allow the restoration of NO_3^- transport, although with some delay. This indicates that *PtNPF1* is an integrated part of a complex cellular network that enables diatoms to react properly to changing environmental conditions, to save nutrients and energy in times of plenty, the so-called luxury uptake, and to meet future changing demands.

Understanding the signalling pathways that transduce intra- and extracellular N signals into physiological responses is an active field of research, and can help to explain the reason of diatom success in the fluctuating and changing oceanic environment. Moreover, N metabolism in diatoms is highly complex, also considering the chimeric nature of diatom genomes and the genetic redundancy occurring in the regulation of NO_3^- uptake, storage and reallocation machinery.

In this context, we provide more insights into the role of the vacuole in diatoms and on the mechanism of vacuolar NO_3^- efflux, proposing PtNPF1 as one of the main actors regulating such processes. Its functional characterization represents an important brick that can help reconstruct the complex N metabolism in diatoms and to shed light on the diatom vacuole function. However, many indicators, such as the recovery speed of the phenotype indicate many key players have yet to be identified, so this work would be also an invitation to further investigate this interesting and ecologically relevant feature of the cell.

Acknowledgements

Anna Santin was supported by a PhD fellowship funded by the Open University – Stazione Zoologica Anton Dohrn PhD programme. This research was funded by the Gordon and Betty Moore Marine Microbial Initiative, grant no. 7978, by the European Union's Horizon 2020 research and innovation programme ASSEMBLE Plus, project no. 730984, and by the Italian Ministry of University and Research MUR, Italy, under the Progetti di ricerca di Rilevante Interesse Nazionale, Next Generation EU PRIN, project no. 202295S3WC. [Correction added on 25 January 2024, after first online publication: the funding details in the preceding sentence have been updated.] Laura Morales de los Ríos was supported by a post-doctoral fellowship funded by the Alfonso Martín Escudero Foundation. The authors wish to thank the SZN Advanced Microscopy facility, the SZN Sequencing and Molecular Analyses facility and Dr Angela Falciatore (Institut de Biologie Physico-Chimique, CNRS Sorbonne Université, Paris) for critical suggestions.

Competing interests

None declared.

Author contributions

AS, MIF and AR designed research. AS, MTR, LMDLR and AR performed research. BL and MIF contributed new reagents or analytical tools. AS, MTR, LMDLR, MC, MRA, BL, MIF and AR analysed data. AS and AR wrote the first draft of the paper. AS, MTR, MC, MRA, MIF and AR reviewed the paper.

ORCID

Maurizio Chiurazzi https://orcid.org/0000-0003-2023-9572
Maurizio Ribera d'Alcalà https://orcid.org/0000-0002-5492-9961
Maria Immacolata Ferrante https://orcid.org/0000-0002-8102-8018
Benoît Lacombe https://orcid.org/0000-0001-9924-3093
Laura Morales de los Ríos https://orcid.org/0000-0003-4278-8695
Alessandra Rogato https://orcid.org/0000-0002-0373-9076
Monia Teresa Russo https://orcid.org/0000-0003-2001-5384
Anna Santin https://orcid.org/0000-0002-2950-7046

Data availability

The authors confirm that the data supporting the findings of this study are available within the article and its Supporting Information. Additional Supporting Information may be found in the online version of this article.

References

Behrenfeld MJ, Halsey KH, Boss E, Karp-Boss L, Milligan AJ, Peers G. 2021. Thoughts on the evolution and ecological niche of diatoms. *Ecological Monographs* **91**: e01457.

Bender SJ, Durkin CA, Berthiaume CT, Morales RL, Armbrust EV. 2014. Transcriptional responses of three model diatoms to nitrate limitation of growth. *Frontiers in Marine Science* **1**: 1–15.

Bonifacino JS, Traub LM. 2003. Signals for sorting of transmembrane proteins to endosomes and lysosomes. *Annual Review of Biochemistry* **72**: 395–447.

Busseni G, Rocha Jimenez Vieira F, Amato A, Pelletier E, Pierella Karlusich JJ, Ferrante MI, Wincker P, Rogato A, Bowler C, Sanges R *et al.* 2019. Meta-omics reveals genetic flexibility of diatom nitrogen transporters in response to environmental changes. *Molecular Biology and Evolution* **36**: 2522–2535.

Daboussi F, Leduc S, Maréchal A, Dubois G, Guyot V, Perez-Michaut C, Amato A, Falciatore A, Juillerat A, Beurdeley M *et al.* 2014. Genome engineering empowers the diatom *Phaeodactylum tricornutum* for biotechnology. *Nature Communications* **5**: 3831.

Dell'Aquila G, Zauner S, Heimerl T, Kahnt J, Samel-Gondesen V, Runge S, Hempel F, Maier UG. 2020. Mobilization and cellular distribution of phosphate in the diatom *Phaeodactylum tricornutum*. *Frontiers in Plant Science* **11**: 579.

Dortch Q. 1982. Effect of growth conditions on accumulation of internal nitrate, ammonium, amino acids, and protein in three marine diatoms. *Journal of Experimental Marine Biology and Ecology* **61**: 243–264.

Dortch Q, Clayton JR, Thoresen SS, Cleveland JS, Bressler SL, Ahmed SI. 1985. Nitrogen storage and use of biochemical indices to assess nitrogen deficiency and growth rate in natural plankton populations. *Journal of Marine Research* **43**: 437–464.

Edelman GM, Gally JA. 2001. Degeneracy and complexity in biological systems. *Proceedings of the National Academy of Sciences, USA* **98**: 13763–13768.

Efeyan A, Comb WC, Sabatini DM. 2015. Nutrient sensing mechanisms and pathways. *Nature* **517**: 302–310.

Falciatore A, Casotti R, Leblanc C, Abrescia C, Bowler C. 1999. Transformation of nonselectable reporter genes in marine diatoms. *Marine Biotechnology* **1**: 239–251.

Fraisier V, Gojon A, Tillard P, Daniel-Vedele F. 2000. Constitutive expression of a putative high-affinity nitrate transporter in *Nicotiana plumbaginifolia*: evidence for post-transcriptional regulation by a reduced nitrogen source. *The Plant Journal* **23**: 489–496.

Gerasimaitė R, Sharma S, Desfougères Y, Schmidt A, Mayer A. 2014. Coupled synthesis and translocation restrains polyphosphate to acidocalcisome-like vacuoles and prevents its toxicity. *Journal of Cell Science* **127**: 159772.

Gibson DG, Glass JI, Lartigue C, Noskov VN, Chuang R-Y, Algire MA, Benders GA, Montague MG, Ma L, Moodie MM *et al.* 2010. Creation of a bacterial cell controlled by a chemically synthesized genome. *Science* **329**: 52–56.

Gibson DG, Young L, Chuang R-Y, Venter JC, Hutchison CA, Smith HO. 2009. Enzymatic assembly of DNA molecules up to several hundred kilobases. *Nature Methods* **6**: 343–345.

Glibert PM, Wilkerson FP, Dugdale RC, Raven JA, Dupont CL, Leavitt PR, Parker AE, Burkholder JM, Kana TM. 2016. Pluses and minuses of ammonium and nitrate uptake and assimilation by phytoplankton and implications for productivity and community composition, with emphasis on nitrogen-enriched conditions: pluses and minuses of NH_4^+ and NO_3^-. *Limnology and Oceanography* **61**: 165–197.

Gojon A, Krouk G, Perrine-Walker F, Laugier E. 2011. Nitrate transceptor(s) in plants. *Journal of Experimental Botany* **62**: 2299–2308.

Guillard RRL. 1975. Culture of phytoplankton for feeding marine invertebrates. In: Smith WL, Chanley MH, eds. *Culture of marine invertebrate animals*. Boston, MA, USA: Springer, 29–60.

Haeussler M, Schönig K, Eckert H, Eschstruth A, Mianné J, Renaud J-B, Schneider-Maunoury S, Shkumatava A, Teboul L, Kent J *et al.* 2016. Evaluation of off-target and on-target scoring algorithms and integration into the guide RNA selection tool CRISPOR. *Genome Biology* **17**: 148.

He Y-N, Peng J-S, Cai Y, Liu D-F, Guan Y, Yi H-Y, Gong J-M. 2017. Tonoplast-localized nitrate uptake transporters involved in vacuolar nitrate efflux and reallocation in *Arabidopsis*. *Scientific Reports* **7**: 6417.

Helliwell KE. 2023. Emerging trends in nitrogen and phosphorus signalling in photosynthetic eukaryotes. *Trends in Plant Science* **28**: 344–358.

Hildebrand M, Dahlin K, Volcani BE. 1998. Characterization of a silicon transporter gene family in *Cylindrotheca fusiformis*: sequences, expression analysis, and identification of homologs in other diatoms. *Molecular and General Genetics* **260**: 480–486.

Huang W, Haferkamp I, Lepetit B, Molchanova M, Hou S, Jeblick W, Río Bártulos C, Kroth PG. 2018. Reduced vacuolar β-1,3-glucan synthesis affects carbohydrate metabolism as well as plastid homeostasis and structure in *Phaeodactylum tricornutum*. *Proceedings of the National Academy of Sciences, USA* **115**: 4791–4796.

Huang W, Río Bártulos C, Kroth PG. 2016. Diatom vacuolar 1,6-β-transglycosylases can functionally complement the respective yeast mutants. *Journal of Eukaryotic Microbiology* **63**: 536–546.

Jaubert M, Duchêne C, Kroth PG, Rogato A, Bouly J-P, Falciatore A. 2022. Sensing and signalling in diatom responses to abiotic cues. In: Falciatore A, Mock T, eds. *The molecular life of diatoms*. Cham, Switzerland: Springer International Publishing, 607–639.

Kamp A, de Beer D, Nitsch JL, Lavik G, Stief P. 2011. Diatoms respire nitrate to survive dark and anoxic conditions. *Proceedings of the National Academy of Sciences, USA* **108**: 5649–5654.

Knight MJ, Senior L, Nancolas B, Ratcliffe S, Curnow P. 2016. Direct evidence of the molecular basis for biological silicon transport. *Nature Communications* **7**: 11926.

Kooistra WHCF, Gersonde R, Medlin LK, Mann DG. 2007. The origin and evolution of the diatoms: their adaptation to a planktonic existence. In: Falkowski P, Knoll AH, eds. *Evolution of primary producers in the sea*. Burlington, MA, USA: Elsevier Inc., 207–249.

Kumar A, Sandhu N, Kumar P, Pruthi G, Singh J, Kaur S, Chhuneja P. 2022. Genome-wide identification and *in silico* analysis of NPF, NRT2, CLC and SLAC1/SLAH nitrate transporters in hexaploid wheat (*Triticum aestivum*). *Scientific Reports* **12**: 11227.

Lamig L, Moreno S, Álvarez JM, Gutiérrez RA. 2022. Molecular mechanisms underlying nitrate responses in plants. *Current Biology* **32**: R433–R439.

Laugier E, Bouguyon E, Mauriès A, Tillard P, Gojon A, Lejay L. 2012. Regulation of high-affinity nitrate uptake in roots of *Arabidopsis* depends predominantly on posttranscriptional control of the NRT2.1/NAR2.1 transport system. *Plant Physiology* **158**: 1067–1078.

Léran S, Noguero M, Corratgé-Faillie C, Boursiac Y, Brachet C, Lacombe B. 2020. Functional characterization of the *Arabidopsis* abscisic acid transporters NPF4.5 and NPF4.6 in *Xenopus* oocytes. *Frontiers in Plant Science* **11**: 144.

Lomas MW, Glibert PM. 2000. Comparison of nitrate uptake, storage, and reduction in marine diatoms and flagellates. *Journal of Phycology* **36**: 903–913.

Longo A, Miles NW, Dickstein R. 2018. Genome mining of plant NPFs reveals varying conservation of signature motifs associated with the mechanism of transport. *Frontiers in Plant Science* **9**: 1668.

McCarthy JK, Smith SR, McCrow JP, Tan M, Zheng H, Beeri K, Roth R, Lichtle C, Goodenough U, Bowler CP *et al.* 2017. Nitrate reductase knockout uncouples nitrate transport from nitrate assimilation and drives repartitioning of carbon flux in a model pennate diatom. *Plant Cell* **29**: 2047–2070.

Mikaelyan AS, Pautova LA, Chasovnikov VK, Mosharov SA, Silkin VA. 2015. Alternation of diatoms and coccolithophores in the north-eastern Black Sea: a response to nutrient changes. *Hydrobiologia* **755**: 89–105.

Miller AJ, Zhou JJ. 2000. Xenopus oocytes as an expression system for plant transporters. *Biochimica et Biophysica Acta (BBA) - Biomembranes* **1465**: 343–358.

Noguchi T, Hayashi Y. 2014. Vacuoles and Storage Organelles. In: Noguchi T, Kawano S, Tsukaya H, Matsunaga S, Sakai A, Karahara I, Hayashi Y, eds. *Atlas of plant cell structure*. Tokyo, Japan: Springer, 89–106.

Nymark M, Sharma AK, Sparstad T, Bones AM, Winge P. 2016. A CRISPR/Cas9 system adapted for gene editing in marine algae. *Scientific Reports* **6**: 24951.

Park M, Song K, Reichardt I, Kim H, Mayer U, Stierhof Y-D, Hwang I, Jürgens G. 2013. *Arabidopsis* μ-adaptin subunit AP1M of adaptor protein complex 1 mediates late secretory and vacuolar traffic and is required for

growth. *Proceedings of the National Academy of Sciences, USA* **110**: 10318–10323.

Pfaffl MW, Horgan GW, Dempfle L. 2002. Relative expression software tool (REST©) for group-wise comparison and statistical analysis of relative expression results in real-time PCR. *Nucleic Acids Research* **30**: 10–336.

Pii Y, Alessandrini M, Dall'Osto L, Guardini K, Prinsi B, Espen L, Zamboni A, Varanini Z. 2016. Time-resolved investigation of molecular components involved in the induction of NO_3^- high affinity transport system in maize roots. *Frontiers in Plant Science* **7**: 1657.

Raven JA, Beardall J. 2022. Evolution of phytoplankton in relation to their physiological traits. *Journal of Marine Science and Engineering* **10**: 194.

Rogato A, Amato A, Iudicone D, Chiurazzi M, Ferrante MI, d'Alcalà MR. 2015. The diatom molecular toolkit to handle nitrogen uptake. *Marine Genomics* **24**: 95–108.

Rosenwasser S, Graff van Creveld S, Schatz D, Malitsky S, Tzfadia O, Aharoni A, Levin Y, Gabashvili A, Feldmesser E, Vardi A. 2014. Mapping the diatom redox-sensitive proteome provides insight into response to nitrogen stress in the marine environment. *Proceedings of the National Academy of Sciences, USA* **111**: 2740–2745.

Russo MT, Santin A, Rogato A, Ferrante MI. 2022. Optimized proteolistic protocol for the delivery of the Cas9 protein in *Phaeodactylum tricornutum*. *Methods in Molecular Biology* **2498**: 327–336.

Russo MT, Santin A, Zuccarotto A, Leone S, Palumbo A, Ferrante MI, Castellano I. 2023. The first genetic engineered system for ovothiol biosynthesis in diatoms reveals a mitochondrial localization for the sulfoxide synthase OvoA. *Open Biology* **13**: 220309.

Sabatino V, Russo MT, Patil S, d'Ippolito G, Fontana A, Ferrante MI. 2015. Establishment of genetic transformation in the sexually reproducing diatoms *Pseudo-nitzschia multistriata* and *Pseudo-nitzschia arenysensis* and inheritance of the transgene. *Marine Biotechnology* **17**: 452–462.

Santin A, Caputi L, Longo A, Chiurazzi M, Ribera d'Alcalà M, Russo MT, Ferrante MI, Rogato A. 2021. Integrative omics identification, evolutionary and structural analysis of low affinity nitrate transporters in diatoms, diNPFs. *Open Biology* **11**: 200395.

Schindelin J, Arganda-Carreras I, Frise E, Kaynig V, Longair M, Pietzsch T, Preibisch S, Rueden C, Saalfeld S, Schmid B *et al.* 2012. Fiji: an open-source platform for biological-image analysis. *Nature Methods* **9**: 676–682.

Schreiber V, Dersch J, Puzik K, Bäcker O, Liu X, Stork S, Schulz J, Heimerl T, Klingl A, Zauner S *et al.* 2017. The central vacuole of the diatom *Phaeodactylum tricornutum*: identification of new vacuolar membrane proteins and of a functional di-leucine-based targeting motif. *Protist* **168**: 271–282.

Serif M, Dubois G, Finoux A-L, Teste M-A, Jallet D, Daboussi F. 2018. One-step generation of multiple gene knock-outs in the diatom *Phaeodactylum tricornutum* by DNA-free genome editing. *Nature Communications* **9**: 3924.

Shebanova A, Ismagulova T, Solovchenko A, Baulina O, Lobakova E, Ivanova A, Moiseenko A, Shaitan K, Polshakov V, Nedbal L *et al.* 2017. Versatility of the green microalga cell vacuole function as revealed by analytical transmission electron microscopy. *Protoplasma* **254**: 1323–1340.

Smith SR, Dupont CL, McCarthy JK, Broddrick JT, Oborník M, Horák A, Füssy Z, Cihlář J, Kleessen S, Zheng H *et al.* 2019. Evolution and regulation of nitrogen flux through compartmentalized metabolic networks in a marine diatom. *Nature Communications* **10**: 4552.

Stief P, Kamp A, de Beer D. 2013. Role of diatoms in the spatial-temporal distribution of intracellular nitrate in intertidal sediment. *PLoS ONE* **8**: e73257.

Stief P, Schauberger C, Lund MB, Greve A, Abed RMM, Al-Najjar MAA, Attard K, Bonaglia S, Deutzmann JS, Franco-Cisterna B *et al.* 2022. Intracellular nitrate storage by diatoms can be an important nitrogen pool in freshwater and marine ecosystems. *Communications Earth & Environment* **3**: 154.

Tan MHY. 2020. *A multi-level study of regulation in the model pennate diatom,* Phaeodactylum tricornutum, PhD thesis. San Diego, CA, USA: University of California San Diego.

Tsutsumi E, Matsuno T, Itoh S, Zhang J, Senjyu T, Sakai A, Lee K, Yanagimoto D, Yasuda I, Ogawa H *et al.* 2020. Vertical fluxes of nutrients enhanced by strong turbulence and phytoplankton bloom around the ocean ridge in the Luzon Strait. *Scientific Reports* **10**: 17879.

Tuerena RE, Williams RG, Mahaffey C, Vic C, Green JAM, Naveira-Garabato A, Forryan A, Sharples J. 2019. Internal tides drive nutrient fluxes into the deep chlorophyll maximum over mid-ocean ridges. *Global Biogeochemical Cycles* **33**: 995–1009.

Wang S, Sirbu D, Thomsen L, Kuhnert N, Ullrich MS, Thomsen C. 2019. Comparative lipidomic studies of *Scenedesmus* sp. (Chlorophyceae) and *Cylindrotheca closterium* (Bacillariophyceae) reveal their differences in lipid production under nitrogen starvation. *Journal of Phycology* **55**: 1246–1257.

Yan H, Huang W, Yan C, Gong X, Jiang S, Zhao Y, Wang J, Shi Y. 2013. Structure and mechanism of a nitrate transporter. *Cell Reports* **3**: 716–723.

Supporting Information

Additional Supporting Information may be found online in the Supporting Information section at the end of the article.

Fig. S1 gRNAs design for *Ptnpf1* knock-out mutants generation.

Fig. S2 PtNPF1 amino acid sequence with the predicted vacuole signal peptide at the N-terminus.

Fig. S3 PCR showing amplification of two fragments from *Lhcf2* promoter to *PtNPF1* and from *PtNPF1* to *YFP* in wild-type and cells transformed with Lhcf2p-PtNPF1-YFP-Lhcf1t plasmid.

Fig. S4 Screening and fluorescent GFP signal of positive *Phaeodactylum tricornutum* clones.

Fig. S5 ^{15}N-nitrate accumulation in *Xenopus laevis* oocytes.

Fig. S6 Morphological parameters and intracellular NO_3^- content of *Phaeodactylum tricornutum* wild-type, *Ptnpf1* knock-out mutant KO 2.9 and *PtNPF1* overexpressing strain OE 4 after different days of N starvation, namely 0, 2, 4 and 7 d.

Fig. S7 Intracellular NO_3^- content in *Phaeodactylum tricornutum* wild-type, *Ptnpf1* knock-out mutant KO 2.9 and *PtNPF1* overexpressing strain OE 4 cells grown in $NaNO_3$ and NH_4Cl as alternative N sources in the medium for 4 d.

Fig. S8 *Phaeodactylum tricornutum* wild-type and *Ptnpf1* knock-out mutants schemes and chromatograms showing Cas9 different effects on the two KO alleles.

Fig. S9 Growth curves of *Phaeodactylum tricornutum* wild-type and *Ptnpf1* knock-out mutants in different NO_3^- concentrations and N sources.

Fig. S10 Growth phenotype in *Phaeodactylum tricornutum* wild-type, *Ptnpf1* knock-out mutants and an additional knock-out mutant.

Methods S1 ^{15}N-nitrate accumulation assay in *Xenopus laevis* oocytes.

Table S1 List of primers used for plasmid construction, crRNAs designed for CRISPR/Cas9 proteolistic transformation (with PAM sequence underlined), primers used for overexpressing and knock-out mutants screening, and primers used for qPCRs.

Table S2 Number of experiments performed, and number of cells observed through confocal microscopy to determine morphological parameters, per each condition and per each strain.

Table S3 Predicted subcellular localization of PtNRT2s, using LocTree3 online tool (https://rostlab.org/services/loctree3) via homology-based inference between proteins of known localization.

Please note: Wiley is not responsible for the content or functionality of any Supporting Information supplied by the authors. Any queries (other than missing material) should be directed to the *New Phytologist* Central Office.